Engineering Polymer Microparticles by Droplet Microfluidics

Christophe A. Serra[1]*, Ikram U. Khan[1,2,3], ZhenQi Chang[1], Michel Bouquey[1], René Muller[1], Isabelle Kraus[4], Marc Schmutz[5], Thierry Vandamme[2], Nicolas Anton[2], Christian Ohm[6], Rudolf Zentel[6], Andrea Knauer[7] and Michael Köhler[7]

[1]*Groupe d'Intensification et d'Intégration des Procédés Polymères (G2IP), Institut de Chimie et Procédés pour l'Énergie, l'Environnement et la Santé (ICPEES) — UMR 7515 CNRS, École Européenne de Chimie, Polymères et Matériaux (ECPM), Université de Strasbourg (UdS), 25 rue Becquerel, F-67087 Strasbourg, France*

[2]*Equipe de Pharmacie Biogalénique, Laboratoire de Conception et Application de Molécules Bioactives — CNRS 7199, Faculté de Pharmacie, Université de Strasbourg (UdS), 74 route du Rhin, BP 60024, F-67401 Illkirch Cedex, France*

[3]*College of Pharmacy, Government College University, Faisalabad, Pakistan*

[4]*Institut de Physique et Chimie des Matériaux de Strasbourg (IPCMS), UMR 7504, CNRS - Université de Strasbourg, 23 rue du Loess, BP 43, F-67034 Strasbourg, France*

[5]*Centre National de la Recherche Scientifique, Institut Charles Sadron (ICS), UPR 22, 23 rue Loess, F-67083 Strasbourg, France*

[6]*Institute of Organic Chemistry, and Excellence Graduate School MAINZ, University of Mainz, Duesbergweg 10–14, D-55099 Mainz, Germany*

[7]*Department of Physical Chemistry and Microreaction Technology, Institute of Physics, Technical University of Ilmenau, Weimarer Straße 32, D-98684 Ilmenau, Germany*

Capillary-based flow-focusing and co-flow microsystems were developed to produce sphere-like polymer microparticles of adjustable sizes in the range of 50 to 600 μm with a narrow size distribution (CV < 5%) and different morphologies (core–shell, janus, and capsules). Rod-like particles whose length was conveniently adjusted between 400 μm and few millimeters were also produced using the same microsystems. Influence of operating conditions (flow rate of the different fluid, microsystem characteristic dimensions, and design) as well as material parameters (viscosity of the different fluids and surface tension) was investigated. Empirical relationships were thus derived from experimental data to predict the microparticle's overall size, shell thickness, or rods length. Besides morphology, microparticles with various compositions were synthesized and their potential applications highlighted: drug-loaded microparticles for new drug delivery strategies, composed inorganic–organic multiscale microparticles for sensorics, and liquid crystalline elastomer microparticles showing an anisotropic reversible shape change upon temperature for thermal actuators or artificial muscles.

Keywords: core–shell, capsule, janus, rod, thermal actuator, composite particles, drug microcarrier

1. Introduction

So far, polymer particles in the range of few microns to hundreds of microns were mainly prepared by either heterogeneous polymerization processes (suspension, supercritical fluid) or by precipitation processes in a non-solvent. However, for this specific range of sizes, these two processes induce a large particle size distribution. On the other hand, new developments in microfabrication techniques have enabled the fabrication of very efficient emulsification microstructured devices which along with capillaries of small dimensions allow emulsifying a fluid in another immiscible fluid. Thus, droplets or bubbles, with an extremely narrow size distribution (the coefficient of variation of the particle size distribution is typically lower than 5%) can be continuously produced and dispersed in a continuous fluid flowing within these microfluidic devices [1]. If the to-be-dispersed phase is composed of a polymerizable liquid, the droplets can be hardened downstream either by thermally or photo-induced polymerization. Over conventional processes, microfluidic-assisted processes offer the possibility not only to precisely control the size of the particle but also its shape, morphology and composition [2–5]. Two different categories of microsystem have been reported for the emulsification of a polymerizable liquid. In the first one, both continuous and dispersed fluids flow inside microchannels, while in the second one, the continuous phase flows inside a tube and the dispersed phase inside a capillary of small dimensions. The emulsification mechanism, which is quite similar for these 2 categories of microsystem, proceeds from the break-up of a liquid thread into droplets when the to-be-dispersed phase is sheared by the continuous and immiscible phase. Three microchannel-based devices are commonly found: the terrace-like microchannel device (Figure 1a), the T-junction microchannel device (Figure 1b), and the flow-focusing microchannel device (Figure 1c). These devices are usually microfabricated, thanks to semiconductor-related-like technologies. Thus, lithographic processes are commonly employed to etch into silicon, glass, or polydimethylsiloxane (PDMS) microchannels in which the continuous and dispersed phases flow. Over capillary-based devices, microchannel-based systems offer some unique features. Microsystems with channel widths as low as few tens of microns can be obtained. Mask lithographic techniques allow for a perfect alignment of the microchannels and complex microstructures. Upstream and downstream functionalities (flow distribution, selective droplets fusion, droplet scissions, etc.) are easily implemented. Finally, chips with multiple microstructures can be designed for increasing the overall production of polymer particles.

Three capillary-based devices are also commonly found: the co-flow capillary device (Figure 1d), the cross-flow capillary device (Figure 1e), and the flow-focusing capillary device (Figure 1f). All the above microchannel-based devices are designed such that the dispersed phase is in direct contact with the wall of the device before being emulsified by the continuous phase. So the device material should be carefully chosen or modified to avoid a phase inversion. This phenomenon is observed when the dispersed phase has a greater affinity for the material than the continuous phase; i.e., when the dispersed phase wets preferentially the walls. As a result, the continuous phase is emulsified by the dispersed phase and droplets of continuous phase are formed. This phase inversion can be avoided by selecting a proper material

* Author for correspondence: serrac@ecpm.u-strasbg.fr

DOI: 10.1556/JFC-D-13-00014

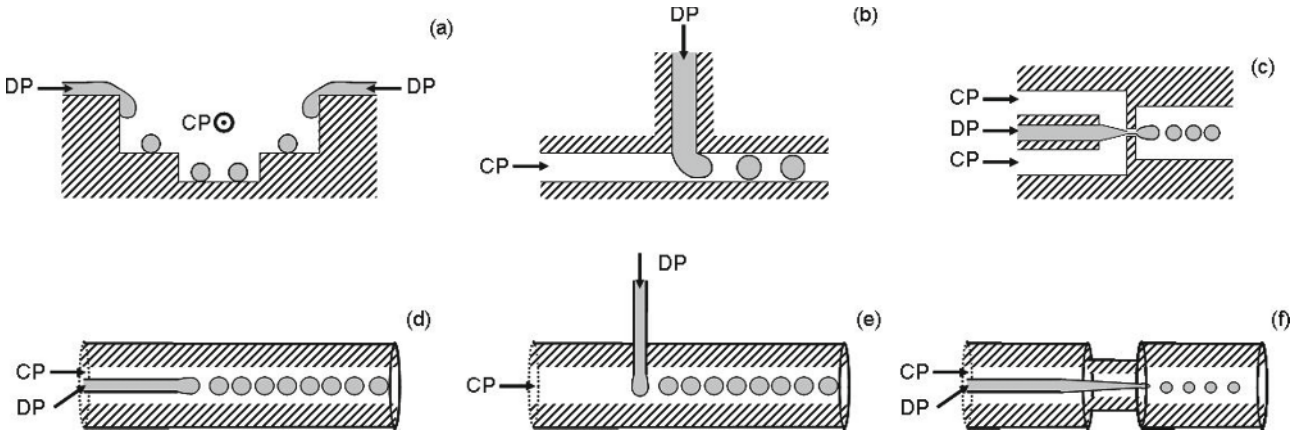

Figure 1. Different microfluidic devices for the emulsification of a liquid monomer. Microchannel-based devices: terrace-like device (a), T-junction device (b), flow-focusing device (c). Capillary-based devices: co-flow device (d), cross-flow device (e), flow-focusing device (f). CP and DP are the continuous and the to-be-dispersed phases, respectively (adapted from ref.[3])

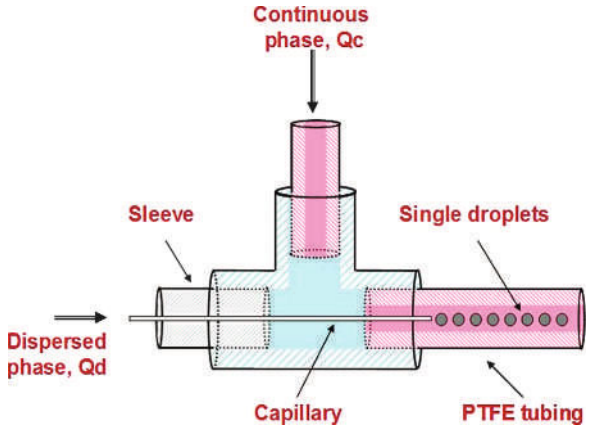

Figure 2. Schematic drawing of the co-flow capillary-based microsystem for the generation of single droplets (adapted from ref.[21])

(hydrophilic for hydrophobic droplets) or by modifying locally the properties of the material at the very location where droplets of dispersed phase are formed. However, the latter procedure requires an additional step in the microfabrication process. Additionally, one can use capillary-based devices to deliver the dispersed phase in the very center line of the continuous phase flow so that the droplets never meet with the device walls. Moreover, these capillary-based devices solve for the clogging of microchannels that can be encountered in the above microchannel-based devices as well as for the possibility to get O/W or W/O emulsion with a single microsystem.

Simple morphologies like beads [3] and capsules [3, 6–8] are easily obtained from the abovementioned microfluidic devices. However, additionally to the greater control over the size, these devices also allow for the production of specific polymer particles, which characteristics (morphology and composition) are likely to be difficult to obtain in conventional batch reactors.

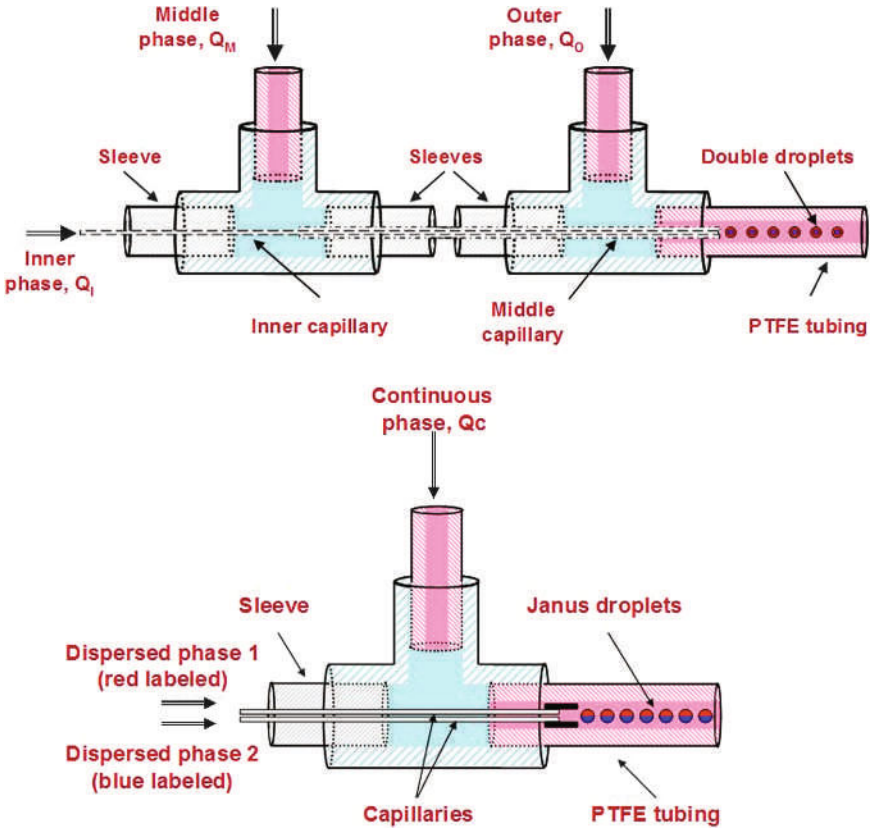

Figure 3. Schematic drawing of the co-flow capillary-based microsystems for the generation of double droplets (top) or janus droplets (bottom) (adapted from ref.[20])

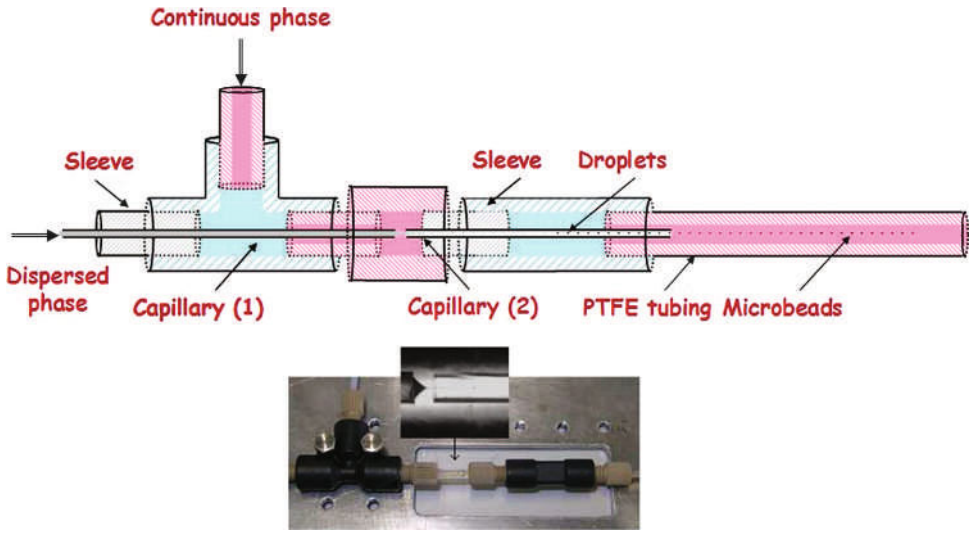

Figure 4. Schematic drawing of the flow-focusing capillary-based microsystem for the generation of single droplets (top) and optical micrograph of the microsystem (bottom). Inset is a magnification of the flow-focusing section (adapted from ref.[24])

For instance, janus particles, composed of two different polymer phases, can be prepared [9–12] and polymer microspheres filled with compound-like magnetic nanoparticles [13], Qdots, or liquid crystals [14, 15] are produced without suffering from the aggregation and sedimentation observed in batch processes. Anisotropic particles can also be produced in such microfluidic devices comprising disk-like [16], rod-like [17], and truncated particles [17] without any additional process for shape forming [19]. Finally, liquid–polymer [18] and polymer–polymer [20] core–shell are obtained from double emulsions.

In the following, we will present how operating parameters can be tuned to produce, in capillary-based co-flow and flow-focusing devices, polymer microparticles with defined size, composition, and morphology. Furthermore, we will emphasize their properties and highlight their potential applications.

2. Materials and Methods

2.1. Capillary-Based Microsystems. Microdroplets and subsequent polymer microparticles were obtained from capillary-based microfluidic devices consisting in different arrangement of capillaries – single (Figure 2), co-axial (Figure 3 top), and side-by-side (Figure 3 bottom) – having small inner diameters (ca. 20–150 μm). Two main devices were developed: a co-flow (Figure 2, Figure 3) and a flow-focusing microsystem (Figure 4). At the capillary tip, the to-be-dispersed phase, composed of a monomer solution admixed with an initiator, is sheared by the continuous phase to form, in the dripping regime, droplets of same volume with a regular frequency up to several tens of Hz. Depending on the capillaries arrangement, single, double, or janus droplets were produced. All microsystems were composed of capillaries with hydrophilic (fused silica tubing, Polymicro Technologies) or hydrophobic (PEEK or PTFE tubings, Upchurch Scientific) inner walls, T-junctions (P-728-01, Upchurch Scientific), and tubing (polytetrafluoroethylene, Fisher Scientific Bioblock).

2.2. Procedures. Depending on the type of microparticle to be synthesized, the dispersed phases were composed of either a hydrophobic monomer (methyl methacrylate, MMA; tri(propylene glycol) diacrylate, TPGA; ethyl acrylate, EA) admixed with an organo soluble photoinitiator (1-hydroxycyclohexyl phenyl ketone, HCPK; Irgacure 907), a crosslinker (dimethacrylate ethylene glycol, DIMAEG), and possibly an organic fluorescent dye (4-octyl-7-(5-octyl-thiophen-2-yl)-benzol [1,2-5]thiadiazole); or a hydrophilic monomer (acrylamide, AA) dissolved in deionized water along with a crosslinker (NN′-methylene-bisacrylamide, MBA) and a water soluble

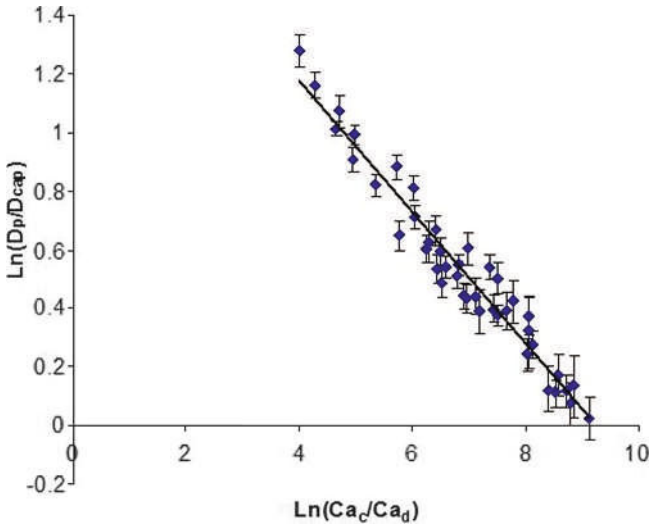

Figure 5. Logarithmic variation of the reduced particle diameter with respect to the continuous to dispersed capillary numbers ratio. The dispersed phase was composed of 92 wt.% MMA, 3 wt.% DIMAEG, and 5 wt.% Irgacure 907, while the continuous phase was an aqueous solution of methyl cellulose of different viscosities (350, 500, 800, 1050, and 1450 cP). Inner capillary diameter was either 110 or 260 μm (adapted from ref.[21])

photoinitiator (Genocure DMHA) or a thermal initiator (ammonium persulfate, APS). The continuous phase was either composed of distilled water admixed with few weight percents of methyl cellulose or carob gum in order to increase the viscosity (typically 2000 cP) and possibly surfactant (SPAN 80) or silicone oils of different viscosities. In some cases, the continuous phase viscosity was increased up to 4000 cP without experiencing any clogging. Dispersed and continuous phases were stored in gas-tight syringes and pumped by digital syringe pumps (PHD 2000, Harvard Apparatus). Once formed, the polymerizable droplets are conveyed by the continuous phase in an outlet tubing and hardened downstream by UV irradiation (UV light source, Lightningcure LC8 at 365 nm, Hamamatsu) into polymeric microparticles. In some cases (core–shell structure), the core was polymerized off-line by thermal-initiated polymerization. For the production of capsules, the dispersed phase was composed of different dichloride acids (sebacoyl and isophtaloyl) in hecadecane, while the continuous phase contained a diamine (hexadecane diamine) and possibly a trifunctional amine (tris(2-aminoethyl)amine, TAEA) for crosslinking.

2.3. Characterization. Formation of droplet was observed under an optical microscope (Eclipse 80i or TS100, Nikon) equipped with a CCD camera (Pike F-032B, AVT) capturing up to 200 fps at a full resolution of 648×488 pixels. Particle

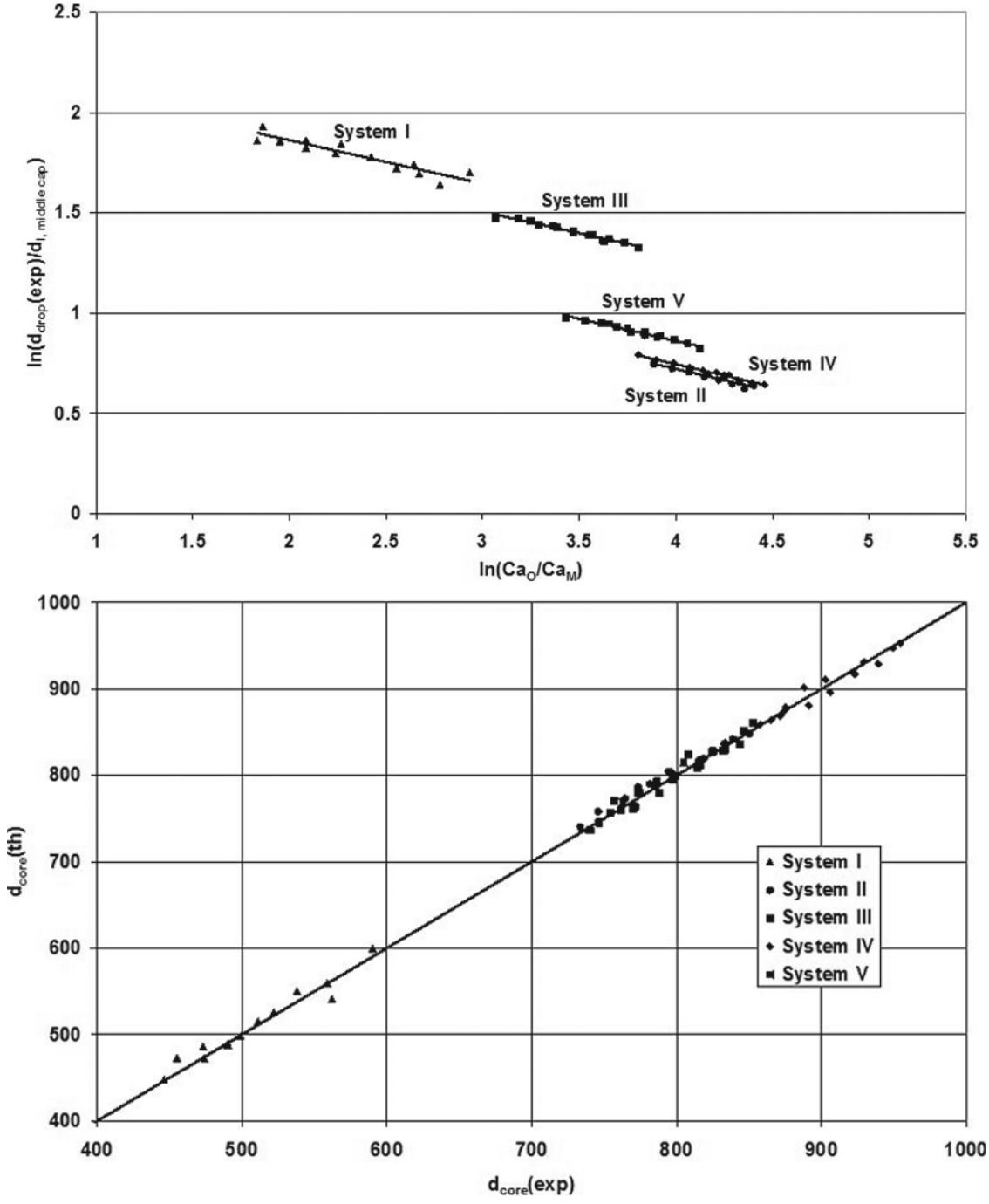

Figure 6. Logarithmic variation of the reduced overall core–shell droplet diameter with respect to the outer to middle capillary numbers ratio (top) and comparison between theoretical and experimental core diameters according to Eq. (3) (bottom). The middle phase was composed of 93 wt.% TPGDA, 3.5 wt.% Span 80, 3.5 wt.% HCPK; the inner phase was composed of 10 wt.% AA, 10 wt.% MBA, 0.15 wt.% APS, and 79.85 wt.% deionized water; the continuous phase was an aqueous solution of methyl cellulose whose viscosity was varied from 500 to 2000 cP. ID and OD of inner and middle capillaries' diameters of the different systems were respectively: system I 20/90 μm and 150/360 μm, system II 75/360 μm and 700/860 μm, system III 100/165 μm and 300/760 μm, system IV 150/360 μm and 700/850 μm, system V 100/360 μm and 530/670 μm, system VI 100/165 μm and 250/360 μm (adapted from ref.[20])

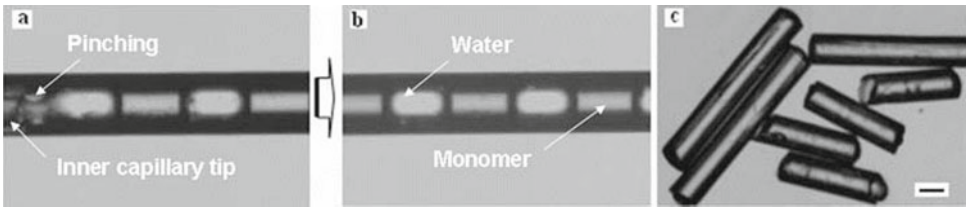

Figure 7. Snapshots of the formation of non-spherical drops (a, b) and the optical microscopy images of the subsequent rod-like poly(TPGDA) particles obtained by varying the ratio of the middle to inner fluid flow rates (c) in microfluidic system VI. Scale bar is 200 μm (adapted from ref. [20])

size and size distribution were obtained by analyzing up to 50 particle optical micrographs by means of an imaging software (Hiris version 3, R&D Vision). Particle shape and surface as well as capsules membrane were observed by scanning electron microscopy (JSM 6380, JEOL; XL FEG/SFEG/Sirion, FEI). Alternatively, scanning electron microscope (SEM) secondary electron images and back-scattered electrons images in chemical Z-contrast (COMPO) were recorded (JSM 6700 F, JEOL) and energy dispersive X-rays spectrometry (EDXS) (Thermo-Noran Vantage) was performed to identify the chemical composition. Composite microbeads were characterized by transmissive, dark-field, and fluorescence microscopy using an optical microscope (Axioplan 2, Zeiss) equipped with mercury high-pressure light source and four filter sets for excitation and emission (in the ranges 300–390/420, 395–440/470, 450–490/515, and 510–560/590). Their inner morphologies were observed by transmission electron microscopy (TECNAI G2 Microscope, FEI) on thin sections. Composite microbeads were first embedded in EPON resin using the standard protocol. Then, after polymerization at 65 °C, the resin blocks were cut using an ULTRA Microtome UCT (Leica) with a diamond knife at a nominal thickness of 50, 100, or 300 nm. The sections were picked up with 200 mesh copper grids and observed with the transmission electron microscopy (TEM) at 200 kV. Images were recorded on an ssCCD camera (Eagle, FEI).

3. Results

3.1. Controlling Droplets and Microparticles Size. Preliminary experiments [21] were conducted to assess the influence of operating parameters – dispersed and continuous velocities, respectively Vd and Vc; internal capillary diameter, d_{cap}; viscosity of dispersed and continuous phases, respectively μ_d and μ_c; and surface tension, γ – on the size of single microparticles. An empirical relation (Eq. (1), Figure 5) was found to fairly well predict the diameter (d_p) of MMA particles obtained from a single capillary microfluidic device (Figure 2):

$$\frac{d_p}{d_{cap}} = 7.92\left(\frac{Ca_c}{Ca_d}\right)^{-0.22} \quad (1)$$

where Ca_c and Ca_d are the continuous and dispersed phase capillary numbers, respectively ($\mu V/\gamma$).

In a further study [20], the same relation was found to hold for the overall diameter of core–shell double droplets (Eq. (2), Figure 6 top) obtained with a co-axial microsystem (Figure 3 top) while the core diameter was fairly well predicted from a single mass balance by Eq. (3) (Figure 6 bottom).

$$\frac{d_{drop}}{d_{I,middle\ cap}} = K\left(\frac{Ca_O}{Ca_M}\right)^{-0.22} \quad (2)$$

$$D_{core} = \sqrt[3]{\frac{Q_I}{Q_I + Q_M}}D_p \quad (3)$$

where d_{drop} is the mean core–shell overall droplet diameter; $d_{I,middle\ cap}$, the middle capillary inner diameter; Ca_O and Ca_M, the capillary numbers of the outer and middle phases, respectively;

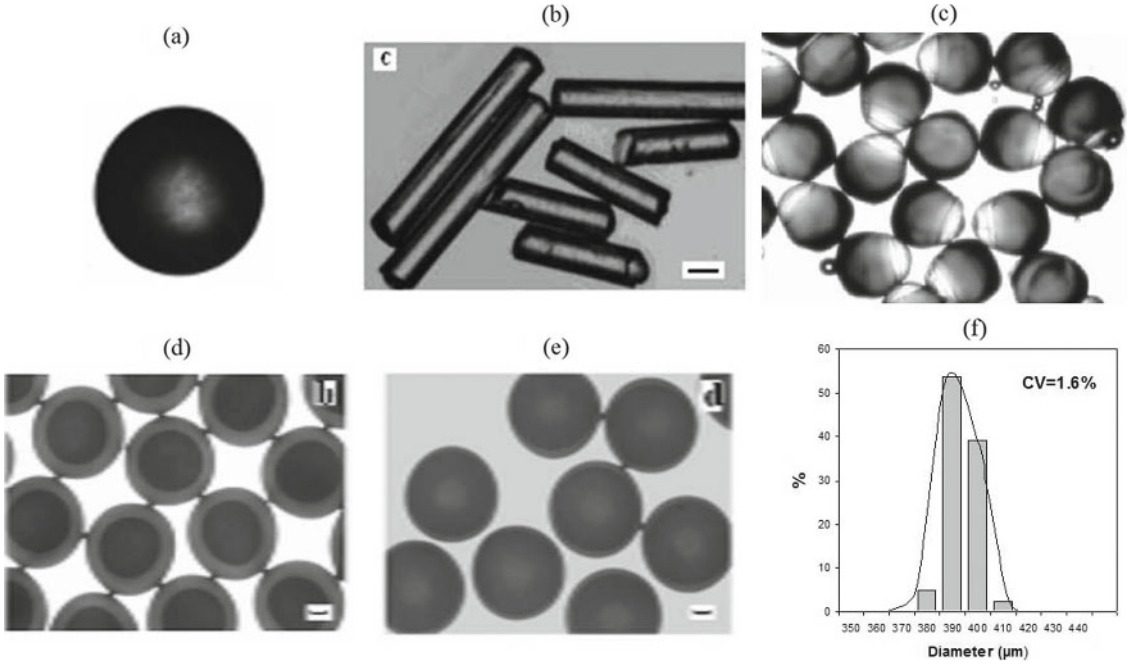

Figure 8. Examples of produced microparticles: (a) poly(TPGDA) microbead, (b) poly(TPGDA) rod-like microparticle, (c) poly(TPGDA)/poly(AA) janus particle, (d, e) poly(AA)–poly(TPGDA) core–shell particle with two different shell thickness, (f) typical particle size histogram. All particles have a diameter ranging from 300 to 500 (adapted from ref.[20])

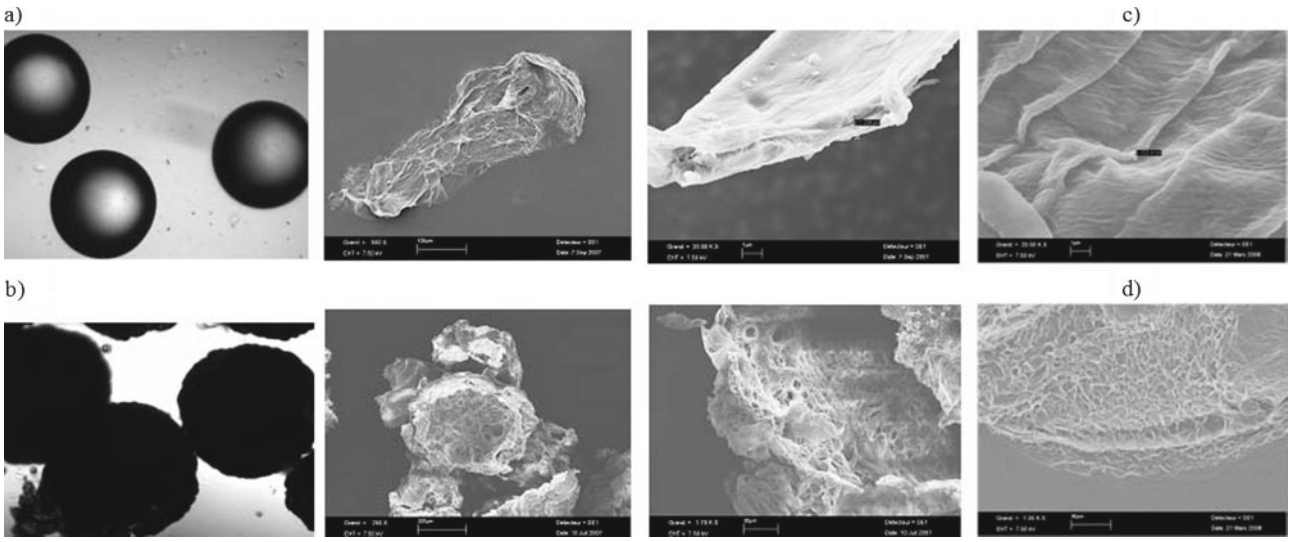

Figure 9. Optical micrographs and SEM micrographs at two different magnifications (from left to right) of capsules obtained from sebacoyl (a) or isophtaloyl (b) chlorides at a molar flow rate of 3.1 mM/min. SEM micrographs of the capsule's membrane obtained from sebacoyl chloride at a molar flow rate of 0.4 mM/min without (c) and with 15 wt.% of a trifunctional amine (d) in the continuous phase

Figure 10. Optical micrographs of a 300-μm crosslinked liquid crystalline particle at different temperatures (adapted from ref.[22])

and Q_I and Q_M, the flow rates of the inner and middle phase, respectively.

Rod-like particles were also produced from a co-axial capillary-based microfluidic device (Figure 3a) having the inner capillary tip inside the middle capillary tip (Figure 7). For that kind of microparticle morphology, their length was found to be highly affected by the ratio of the middle and inner phase flow rates (Eq. (4)).

$$L = 3.23 + 85.62\left(\frac{Q_M}{Q_I}\right)^{1.92} \quad (4)$$

where L is the rod-like particle length.

3.2. Particles with Different Shapes and Morphologies. Application of these capillary-based microsystems allowed the preparation of polymeric microparticles of different shapes (Figure 8a,b): spheres and rods. One can also produce microparticles with different morphologies (Figure 8c–e): janus and core–shell whose shell thickness can be tuned simply by adjusting the operating conditions (mainly continuous and dispersed phase flow rates). Each of the aforementioned microparticles

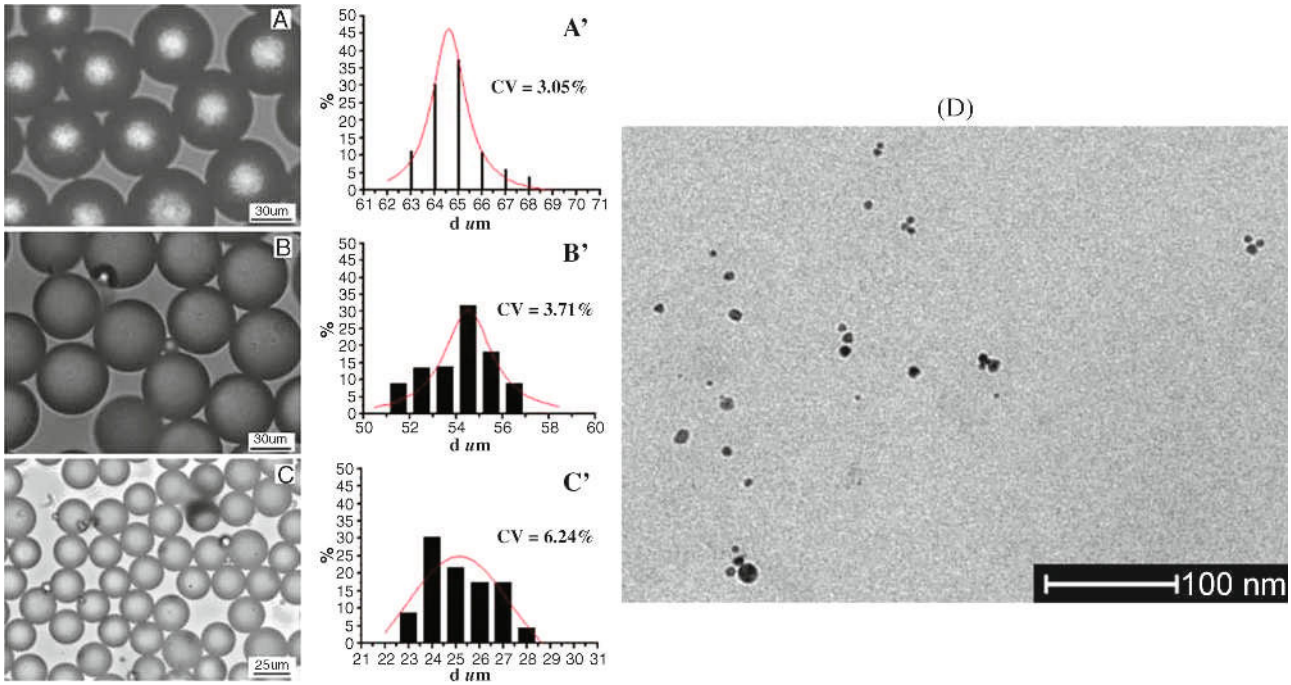

Figure 11. (A–C) Optical microscopy images of nano-Au/poly(TPGDA) composite microbeads obtained for different continuous (Q_C) and dispersed (Q_D) phase flow rates and (A′–D′) their respective particle size distribution; (A, A′), Q_C = 0.1 mL/min, Q_D = 0.001 mL/min; (B, B′), Q_C = 0.15 mL/min, Q_D = 0.001 mL/min; (C, C′), Q_C = 0.18 mL/min, Q_D = 0.0005 mL/min. Continuous phase viscosity was kept constant for all samples (μ_C = 400 cP). (D) TEM micrographs at 200 kV of a poly(TPGDA) microbead containing Au nanoparticles after ultramicrotomy (adapted from ref.[24])

has an extremely narrow size distribution (Figure 8f) as expressed by a low coefficient of variation (typically below 5%).

Capillary-based microsystems were found very convenient to produce polymeric capsules (average size of 300 μm) and to investigate effect of operating and composition parameters on the morphology of the membrane. These parameters can be easily changed, and a small amount as low as 1 mL of the dispersed phase is required to investigate capsules characteristics. More conventional processes for the production of polymeric capsules (batch reactors) lack this versatility, not to mention that a significantly larger amount of reactants are to be used. By using microsystem of Figure 1, we produced droplets of a dichloride acid and hexadecane conveyed by a stream of an aqueous solution. Downstream, a side stream of the continuous phase admixed with a diamine (hexane diamine) merged with the main stream. Upon contact of the dichloride acid and diamine, an interfacial polycondensation reaction took place and resulted in the formation of the capsule polyamide membrane. Morphology of the membrane was first studied by varying the nature of the dichloride acid. Use of sebacoyl chloride resulted in smooth, transparent, and soft capsules with a dense membrane whose thickness was around 1 μm (Figure 9a), while isophtaloyl conducted to irregular, hard, and opaque capsules with a thick (20 μm) and porous membrane (Figure 9a). Molar ratio in-between reactant can be readily adjusted by tuning the volumetric flow rate of the dispersed phase and side stream. By lowering down the molar flow rate of the sebacoyl acid keeping constant that of hexane diamine, an extremely dense membrane was produced (thickness around 250 nm, Figure 9c). Finally, the use of few weight percents of a trifunctional amine (TAEA) acting as a crosslinker allowed to produce even thinner membrane (Figure 9d) whose dense crosslinked network efficiently blocked the diffusion of the reactants towards each other.

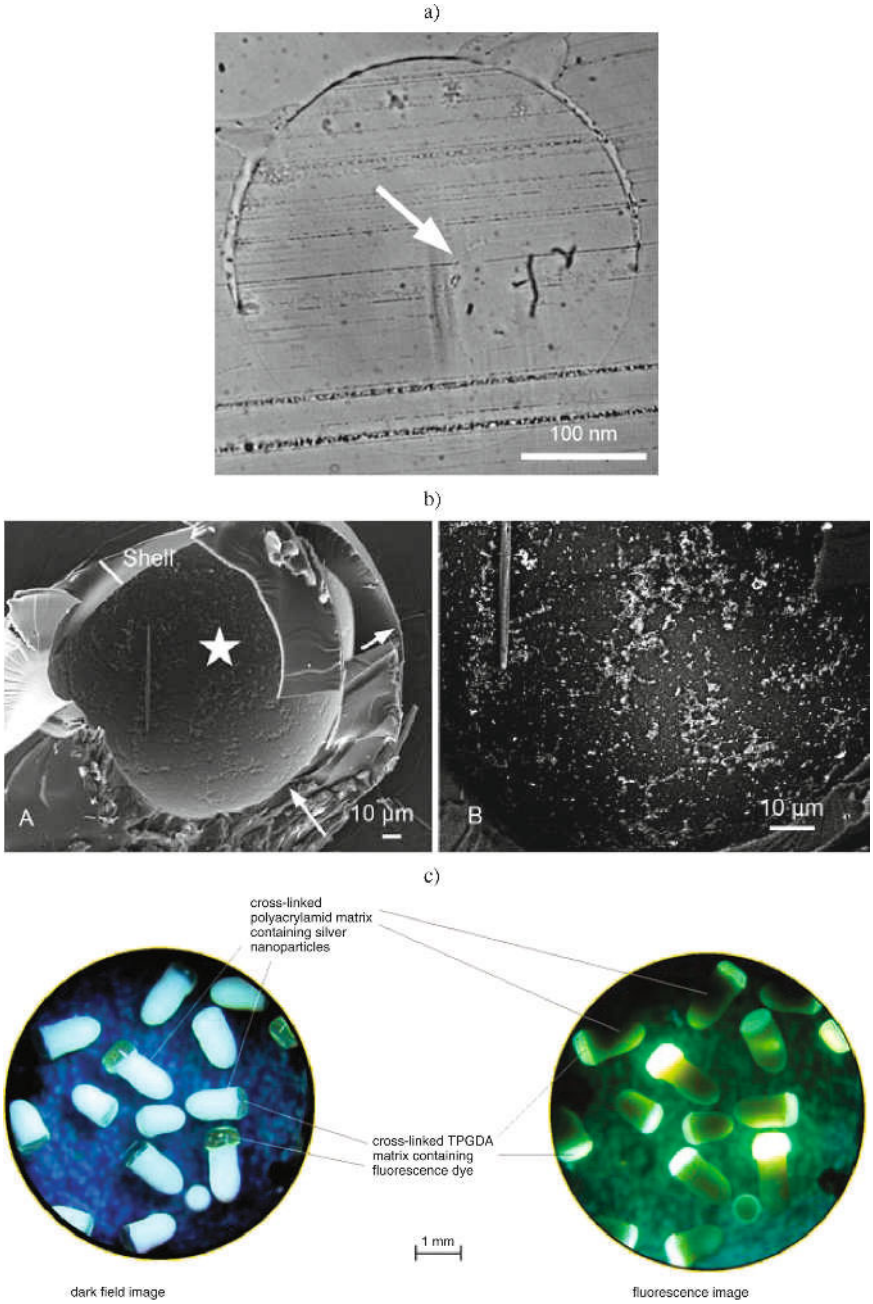

Figure 12. (a) Optical image of an ultramicrotomy cut of a ZnO/ZnO core–shell microparticle. (b) SEM micrograph of an ultramicrotomy cut of a ZnO/Au core–shell microparticle: (A) poly(AA) core (long-white arrow) covered with ZnO nanoparticles aggregates, the white star figures the region investigated by EDX spectroscopy where Zn appears as bright white dots (B). (c) Dark-field microscopic image (left) and fluorescence microscopic image (right) of janus polymer composite microparticles consisting of a fluorescent poly(TPGDA) matrix (mushroom heads) and a light-scattering crosslinked poly(AA) matrix doped with silver nanoprisms (tail) (adapted from ref.[25])

3.3. Particles for Different Applications. The above developed co-flow capillary-based microsystems were used to prepare polymeric materials under the form of spherical or janus-like microparticles. These microparticles exhibit some specific properties which arise from either the narrow size distribution or from their morphology that cannot be achieved when they are prepared by more conventional synthetic methods. Thus, microsystem of Figure 2 was used to produce liquid crystalline microparticles [22, 23], which present upon temperature an anisotropic and reversible shape change (Figure 10) around the nematic–isotropic phase transition temperature. These interesting properties may find application as artificial muscles or valves in microfluidic chips.

$$T = 100°C \quad T = 120\,°C \quad T = 140\,°C \quad T = 100\,°C$$

Inorganic–organic composite microparticles were obtained by emulsification and subsequent polymerization of a monomer phase consisting in TPGDA, Au nanoparticles (13 nm) and HCPK with the microsystem of Figure 4. Due to the increase in the shear rate exerted by the continuous phase on the growing droplet, the flow-focusing device allows the production of smaller particles than its co-flow counterpart. However, we observed that the coefficient of variation is usually higher reflecting the statistical droplet break-off under Rayleigh–Plateau instabilities when the continuous phase flow rate is increased (Figure 11A′–C′). TEM analysis of ultramicrotomic cuts of the obtained microparticles clearly revealed the good dispersion of the Au nanoparticles within the polymeric matrix (Figure 11D) [24].

More recently, by using microsystem of Figure 3a, we produced 300 μm poly(AA)–poly(TPGDA) core–shell microparticles (Figure 12a,b) selectively incorporating Au or ZnO nanoparticles (13 nm for the former and 2 μm for the latter) in the shell or in the core. The specific core–shell morphology was evidenced on an ultramicrotomy cut of 300-nm thickness by SEM analysis (Figure 12a). One clearly observes (black arrow) the core while the presence of ZnO nanoparticles in the core was revealed by EDX spectroscopy (Figure 12b). By arranging two microsystems of Figure 2 in a row, we also obtained in recent past even more complex composite polymeric microparticles. Thus, janus-like microparticles composed of a poly(AA) matrix doped with silver nanoprisms (average size of 24 nm) and a poly(TPGA) matrix containing an organic fluorescent dye were produced [25]. The resulting particles presented strong selective fluorescent properties as shown in Figure 12c. These composite microparticles allow an easy handling of nanoparticles and may find applications in sensorics as the plasmonic properties of encapsulated nanoparticles may be affected by pH, oxygen content, or analyte concentration. Preliminary experiments showed that Ag-nanoparticles-doped poly(AA) microparticles exhibit a strong surface-enhanced Raman spectroscopy (SERS) signal upon contact with ademine concentration as low as 0.1 μM [26].

Finally, drug-loaded microparticles were recently synthesized from microsystem of Figure 2 and composition of the to-be-dispersed phase was changed to modulate the release property of the ketoprofen model drug that was beforehand dissolved in the dispersed phase [27]. As seen in Figure 13a, microparticles'

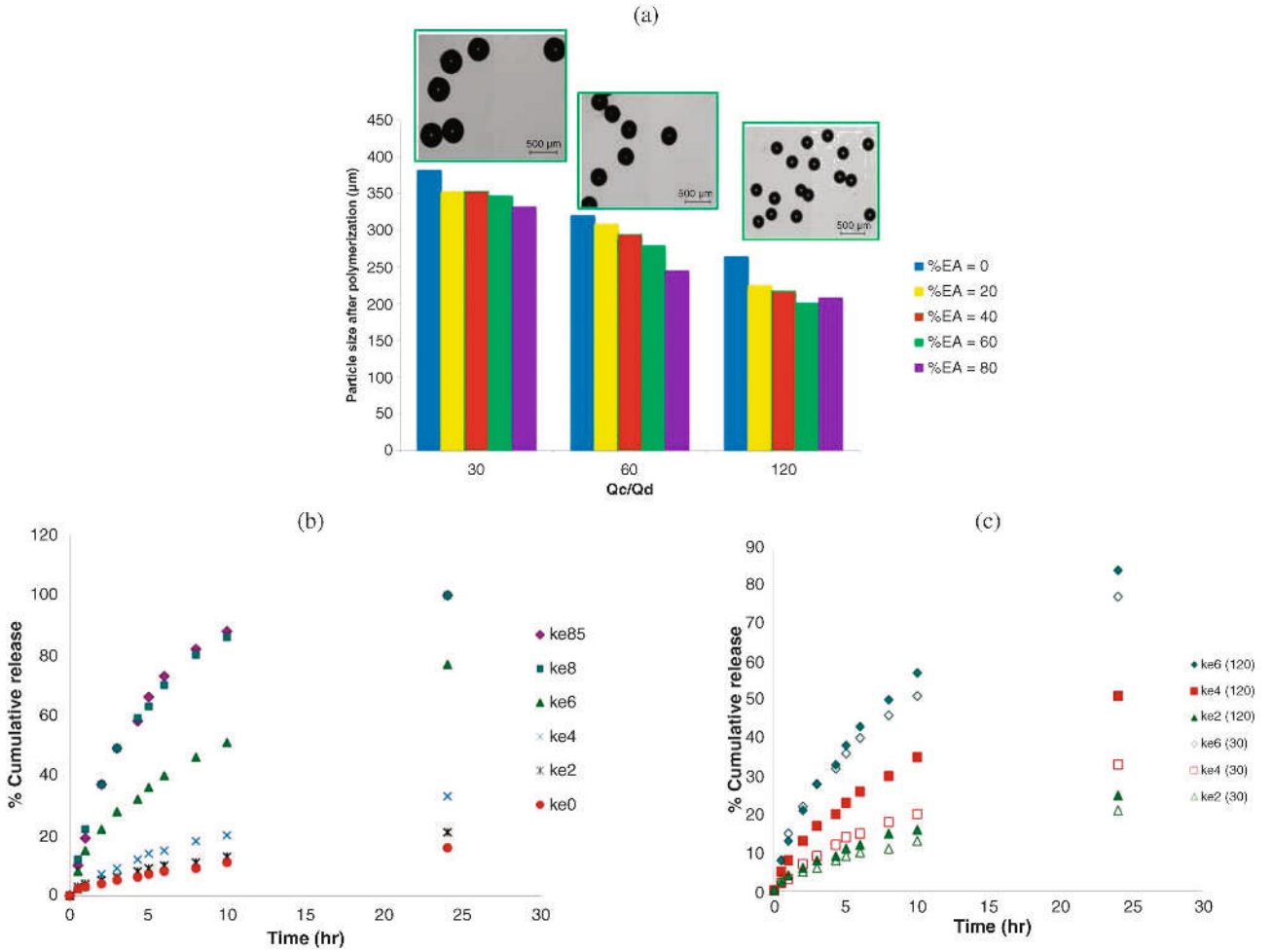

Figure 13. (a) Variation of particles' diameter with respect to continuous to dispersed phase flow rates ratio for different EA weight contents in the EA/TPGDA/ketoprofen dispersed phase. Insets present the corresponding optical micrographs. (b) Cumulative release rate profile versus time for different EA/TPGDA compositions (ke0: 100 % TPGDA, ke2: 20 % EA, ke4: 40 % EA, ke6: 60 % EA, ke8: 80 % EA, ke85: 85 % EA). (c) Influence of continuous to dispersed phase flow rates ratio on cumulative release rate profile (120 stands for $Q_c/Q_d = 120$; 30 stands for $Q_c/Q_d = 30$) (adapted from ref.[27])

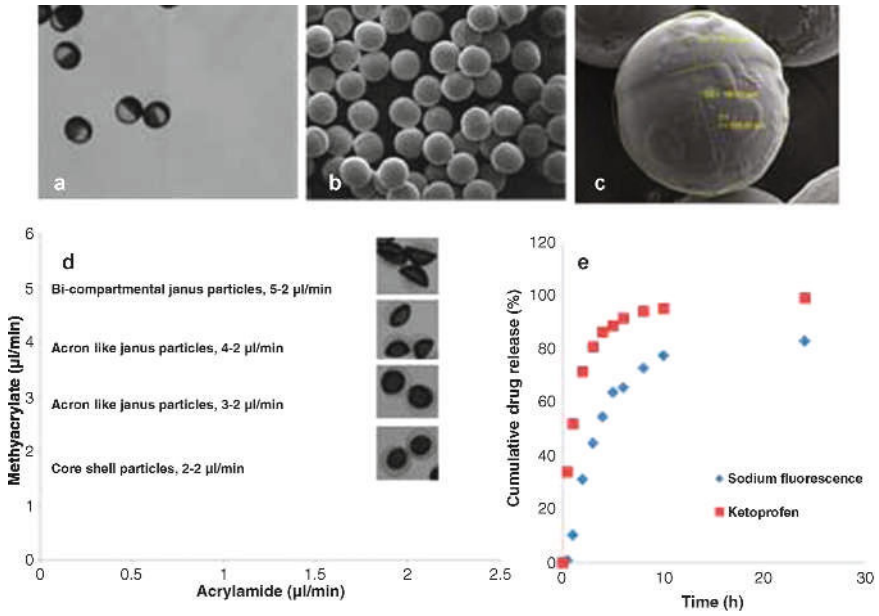

Figure 14. (a) Optical microscopic image of janus particles, (b) SEM micrograph of several janus particles, (c) SEM magnification image of a single janus particle having an overall diameter of 250 µm and comprising two different domains having a diameter of 181 and 76 µm for hydrophobic and hydrophilic portion, respectively, (d) change of morphology of particles as function of the flow rate of two phases, and (e) cumulative percentage release of two active pharmaceutical ingredients over a period of 24 h

diameter varies with respect to the continuous to dispersed phase flow rates ratio accordingly to Eq. (1): the higher the ratio, the smaller are the particles. One also notices that the diameter slightly decreases when the weight content of EA is increased from 0 to 80 % in the EA/TPGDA/ketoprofen dispersed phase. Since the TPGDA is a bifunctional monomer, a large amount of that compound results in a rapid crosslinking of the matrix network leading to a particle size close to the droplet size. Conversely, a large amount of EA (a monofunctional monomer) will result in a volume contraction upon polymerization due to the higher density of the polymer with respect to that of its monomer. As shown in Figure 13b, the higher the weight content of EA in the dispersed phase, the higher is the release rate of the drug. This results from the looseness of the polymer matrix induced by less amount of bifunctional monomer (TPGDA), which favors the surrounding fluid diffusion through the particle and the subsequent transport of the drug. Figure 12c shows the drug release rate for two sets of Qc/Qd. It is observed that the higher this ratio, the higher is the release rate. When the flow rate ratio is increased, smaller particles are formed (Figure 13a), which reduces the drug diffusion path for the existing particle.

Two model drugs, namely ketoprofen (hydrophobic) and sodium fluorescein (hydrophilic), were incorporated in poly (acrylamide)–poly(methyl acrylate) janus particles by using side-by-side capillary setup as mentioned in Figure 3. Janus structure was confirmed by optical and SEM micrographs as shown in Figure 14a,b,c. It was observed that the flow rate of both dispersed phases affect the overall particles morphology. At low flow rate of the MMA phase, one got a core–shell like structure while increasing the flow rate of hydrophobic monomer at constant hydrophilic monomer results in a janus structure (Figure 14d). These janus particles were able to release two molecules, i.e., ketoprofen and sodium fluorescein in a controlled manner over 24 h (Figure 14e).

4. Conclusion

In this work, it was demonstrated that the use of capillary-based microfluidic devices allows for the synthesis of size-, shape-, morphology- and composition-controlled polymer particles in the size range of tens to hundreds of microns without any surfactant or surface treatment. Empirical relationships allow predicting the particle size and core diameter (for core–shell particles) as well as rod-like particle length as a function of the operating parameters. These microsystems were found versatile enough for the generation of oil/water and water/oil emulsions and the subsequent production of microstructured polymer materials like inorganic–organic composite microbeads for potential sensoric applications, reversible anisotropic shape change liquid crystalline microparticles for potential artificial muscles applications, and drug-loaded microparticles for controlled drug delivery applications.

Acknowledgements. Authors acknowledge the French Ministry of Education and Research for having funded this work through the grant ANR n° NT05-1_45715. Authors are grateful to the PHC PROCOPE, through the project n°17900PG, for having supported the student exchange expenditures in-between the research groups. Anne März from Friedrich-Schiller-Universität Jena and Guy Schlatter from the University of Strasbourg are acknowledged for the SERS analysis of Ag-nanoparticles-doped poly(AA) microparticles and SEM micrograph of janus particles, respectively.

References

1. Christopher, G. F.; Anna, S. L. *J. Phys. D: Appl. Phys.* **2007**, *40*, R319–R336.
2. Serra, C. *Handbook of Micro Process Engineering*, Wiley-VCH: Weinheim, **2009**.
3. Serra, C. A.; Chang, Z. *Chem. Eng. Technol.* **2008**, *31* (8), 1099–1115.
4. Hessel, V.; Serra, C.; Löwe, H.; Hadziioannou, G. *Chem. Ing. Tech.* **2005**, 77, 1693–1714.
5. Steinbacher, J. L.; McQuade, D. T. *J. Polym. Sci., Part A: Polym. Chem.* **2006**, *44*, 6505–6533.
6. Malloggi, F.; Pannacci, N.; Attia, R.; Monti, F.; Mary, P.; Willaime, H.; Tabeling, P.; Cabane, B.; Poncet, P. *Langmuir* **2010**, *26* (4), 2369.
7. Hennequin, Y.; Pannacci, N.; Pulido de Torres, C.; Tetradis-Meris, G.; Chapuliot, S.; Bouchaud, E.; Tabeling, P. *Langmuir* **2009**, *25* (14), 7857–7861.
8. Tabeling, P. *Phys. Fluids* **2010**, *22*, 21302.
9. Nie, Z.; Li, W.; Seo, M.; Xu, S.; Kumacheva, E. *J. Am. Chem. Soc.* **2006**, *128*, 9408–9412.
10. Nisisako, T.; Torii, T.; Higuchi, T. *Chem. Eng. J.* **2004**, *101*, 23–29.
11. Nisisako, T.; Torii, T.; Takahashi, T.; Takizawa, Y. *Adv. Mater.* **2006**, *18*, 1152–1156.
12. Shepherd, R. F.; Conrad, J. C.; Rhodes, S. K.; Link, D. R.; Marquez, M.; Weitz, D. A.; Lewis, J. A. *Langmuir* **2006**, *22*, 8618–8622.

13. Kim, J. W.; Utada, A. S.; Fernández-Nieves, A.; Hu, Z.; Weitz, D. A. *Angew. Chem., Int. Ed.* **2007**, *46*, 1819–1822.
14. Xu, S. Q.; Nie, Z.; Seo, M.; Lewis, P.; Kumacheva, E.; Stone, H. A.; Garstecki, P.; Weibel, D. B.; Gitlin, I.; Whitesides, G. M. *Angew. Chem., Int. Ed.* **2005**, *44*, 724–728.
15. Lewis, P. C.; Graham, R. R.; Nie, Z.; Xu, S.; Seo, M.; Kumacheva, E. *Macrolecules* **2005**, *38*, 4536–4538.
16. Dendukuri, D.; Tsoi, K.; Hatton, T. A.; Doyle, P. S. *Langmuir* **2005**, *21*, 2113–2116.
17. Seo, M.; Nie, Z.; Xu, S.; Lewis, P. C.; Kumacheva, E. *Langmuir* **2005**, *21*, 4773–4775.
18. Nie, Z.; Xu, S.; Seo, M.; Lewis, P. C.; Kumacheva, E. *J. Am. Chem. Soc.* **2005**, *127*, 8058–8063.
19. Champion, J. A.; Katare, Y. K.; Mitragotri, S. *Proc. Natl. Acad. Sci. U.S. A.* **2007**, *104* (29), 11901–11904
20. Chang, Z.; Serra, C.; Bouquey, M.; Prat, L.; Hadziioannou, G. *Lab. Chip.* **2009**, *9*, 3007–3011.
21. Serra, C.; Berton, N.; Bouquey, M.; Prat, L.; Hadziioannou, G. *Langmuir* **2007**, *23* (14), 7745–7750.
22. Ohm, C.; Serra, C.; Zentel, R. *Adv. Mater.* **2009**, *21*, 4859–4862.
23. Ohm, C.; Serra, C.; Kraus, I.; Zentel, R. *Adv. Funct. Mater.* **2010**, *20*, 4314–4322.
24. Chang, Z.; Serra, C. A.; Bouquey, M.; Kraus, I.; Li, S.; Köhler, J. M. *Nanotechnology* **2010**, *21* (1), 015605.
25. Knauer, A.; Csáki, A.; Fritzsche, W.; Serra, C. A.; Leclerc, N.; Köhler, J. M. *Chem. Eng. J.* **2013**, *227*, 191–197.
26. Koehler, J. M.; Maerz, A.; Popp, J.; Knauer, A.; Kraus, I.; Faerber, J.; Serra, C. *Anal. Chem.* **2013**, *85* (1), 313–318.
27. Khan, I. U.; Serra, C. A.; Anton, N.; Vandamme, T. *Int. J. Pharm.* **2013**, *441* (1–2), 809–817.